XLVI CILAMCE
VITÓRIA - ES - BRAZIL - 2025
XLVI IBERO-LATIN AMERICAN CONGRESS ON COMPUTATIONAL METHODS IN ENGINEERING

Numerical Simulation of Partially Encased Composite Columns with Recycled Aggregate Concrete

Bruno B. Marques[1], Fernanda G. B. S. Oliveira[1], Ana Lúcia H. C. El Debs[1]

[1]*Dept. of Structural Engineering, University of Sao Paulo*
Avenida Trabalhador São-Carlense - 400,13566-590, São Paulo, Brazil
brunobm@usp.br, fernanda.gabriella@usp.br, analucia@sc.usp.br

Abstract. The construction industry is a significant generator of solid waste, and the use of recycled aggregate concrete (RAC) mitigates environmental impacts. However, its application in partially encased composite (PEC) columns remains poorly explored. This study aims to simulate the structural behavior of PEC columns with RAC, considering coarse aggregate replacement ratios of 0%, 30%, and 50%, to evaluate the impact on their load capacity and axial strain response. The ABAQUS® numerical model was calibrated through experimental results and subsequently extended to include an additional replacement ratio for comparative purposes. The results indicate that the reduction in the mechanical properties of the concrete, associated with the gradual increase in the replacement ratio, resulted in a drop in both the load capacity and stiffness of the elements. Nevertheless, the overall structural response of the PEC columns remained consistent. These findings demonstrate the potential of RAC, showing that partial replacement of natural aggregates with recycled aggregates at low and intermediate substitution ratios maintains satisfactory structural behavior.

Keywords: partially encased composite columns, numerical simulation, recycled aggregate concrete.

1 Introduction

The demand for sustainable resources and effective waste management has driven the reuse and recycling of construction and demolition waste (CDW). As reported by Kalinowska-Wichrowska *et al.* [1], the civil engineering sector accounts for around 40% of global resource consumption, with about one-third attributed to aggregates used in cement-based materials. One mitigation strategy is to incorporate CDW as coarse aggregate in concrete, through partial replacement of natural aggregates with recycled concrete aggregates. Although numerous studies have characterized the properties of recycled aggregate concrete (RAC), the inherent variability in CDW composition still stands as a challenge for the development of consistent normative standards. Combined with irregular quality control among suppliers, this uncertainty limits the broader adoption of RAC. (Silva *et al.* [2]). Recently, the Annex N guidelines introduced in the new version of EN 1992-1-1 [3] enable the partial replacement of natural aggregates by recycled aggregates for structural applications. The α_{RA} parameter, defined as the ratio between the total mass of coarse and fine recycled aggregates and the total mass of aggregates in the mix, governs the application of RAC and can vary between 0.2 and 0.4. Below 0.2, the negative effects of recycled aggregates on the mechanical properties of the concrete are considered negligible. In the Brazilian standard [4], the same parameter is used, but the α_{RA} is limited to 0.2.

Most standards that permit the use of structural RAC restrict application to coarse recycled aggregate within a specified replacement ratio limit, typically requiring at least 90% hardened cement paste and natural aggregate fragments in the recycled concrete aggregate (RCA). Numerous investigations have shown that RAC generally decreases workability (Xiao *et al.* [5],Turi Gerin *et al.* [6]) and mechanical strength (Silva *et al.* [2], Oliveira [7], Adessina *et al.*[8]) compared to conventional concrete. Nevertheless, with appropriate mixing techniques and substitution ratios, the higher water absorption of recycled concrete aggregates can lower the effective water–cement ratio and enhance the interfacial transition zone, occasionally increasing compressive strength (Liu *et al.* [9]). An effective approach to enhance the benefits and ease the limitations of RAC involves its use in composite structural elements.

Prior investigations into RAC in composite columns have predominantly examined concrete-filled steel tubes, where both the protective infill and the confinement effect of the steel enhance structural behavior. Studies of partially encased composite (PEC) columns have focused mainly on natural aggregates (Pereira *et al.*[10], Wang *et al.* [11], Ebadi Jamkhaneh *et al.* [12]), considering both compact and non-compact cross-sections. In compact sections, failure typically involves simultaneous steel yielding and concrete crushing, whereas non-compact sections often exhibit local flange buckling between transverse links coupled with concrete crushing. Wu *et al.* [13] explored PEC columns with non-compact sections using large demolished-concrete lumps (80–125 mm) and found that, although up to 33 % RCA content had minimal effect on peak strength and axial strain, it produced a marked post-peak load drop. Marques [14] investigated the behavior of PEC columns with compact sections using RAC with 30% inclusion of steel fibers and verified that the steel fibers contribute to counteract some of the negative effects of including RCA. Liang *et al.* [15] evaluated RAC-filled PEC columns under axial and eccentric loads after high-temperature exposure, observing that higher replacement ratios delayed steel-web heating, while elevated temperatures induced greater capacity losses than increased RCA content. Despite these contributions, comprehensive data on PEC columns incorporating RAC remains limited. Therefore, this study conducted numerical simulations to investigate the structural behavior of PEC columns with RAC at coarse aggregate replacement ratios of 0 %, 30 % and 50 %, focusing on load capacity and axial strain response.

2 Numerical investigation

Two phases compose the present numerical investigation: (i) calibration of the numerical model according to experimental results; and (ii) variation of the concrete properties to consider different replacement ratios. The experimental results from Pereira *et al.* [10] and Marques [14] allowed for the calibration of the model. Figure 1 shows the test setup used in both studies. Simulations were developed using the ABAQUS® software.

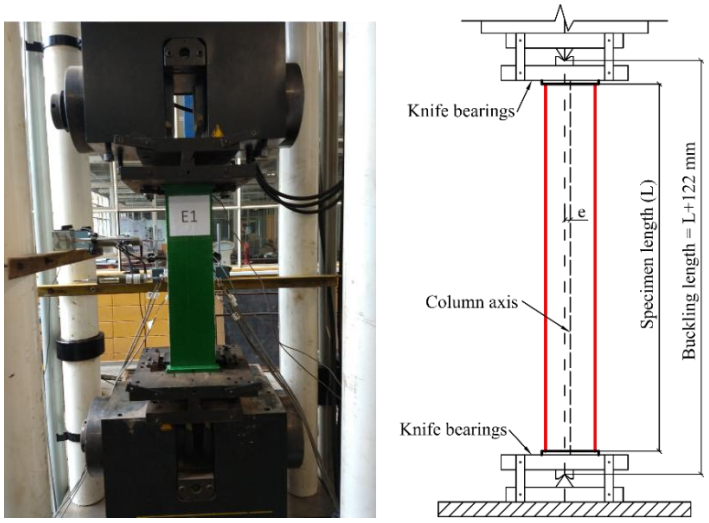


Figure 1 – Experimental test setup (Marques [14])

2.1 Description of the numerical model

The experimental specimens consisted of a W150x22.5 steel profile partially encased in concrete. Figure 2 (a) shows the geometry of the numerical model and the boundary conditions. All the displacements and rotations regarding the z-axis were restricted at the bottom edge. Lateral displacements and rotations in the z-axis were restricted at the top edge, and the load was applied as an axial displacement in the z-direction. The boundary conditions were applied at the reference points (RPs) 1 and 4, which were connected to RPs 2 and 3, respectively, by a coupling constraint. Rigid body constraints connected RPs 2 and 3 to the rigid plates, which were used to distribute the load over the cross-section. The distance between RPs 1 and 4 is equal to the buckling length, as shown in Fig. 1. Figure 2 (b) illustrates the element meshes and the disposal of the steel reinforcement embedded in the concrete. Steel rebars with 8 mm and 6.3 mm composed the longitudinal reinforcement in the studies of Pereira *et al.* [10] and Marques [14], respectively. In both studies, 5 mm rebars were used for the stirrups.

Table 1 shows the properties of each column. Specimens tested by Pereira *et al.* [10] are identified by the prefix "P", while specimens by Marques [14] received the prefix "M". The experimental models encompass two different types of concrete: natural aggregate concrete (NAC) and recycled aggregate concrete with a 30% replacement ratio (RAC30). Table 1 identifies specimens bent regarding the weak (e_x) and strong (e_y) axes, indicating also the accidental eccentricities reported for the axially loaded columns. Additionally, the steel yielding strength (f_y), the concrete compressive strength (f_c), and the longitudinal reinforcement yielding strength (f_s) are also indicated.

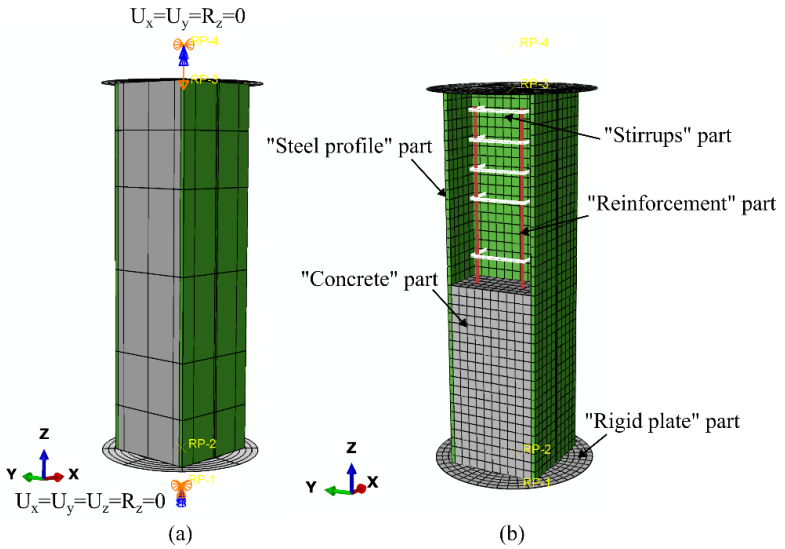


Figure 2 – Numerical model: (a) geometry and boundary conditions and (b) FE meshes

Table 1 – Properties of the experimental models

Specimen	L mm	e_x mm	e_y mm	f_y MPa	f_c MPa	f_s MPa	Concrete type
P-S-RC-0[1]	600	3	-				NAC
P-S-RC-25y	600	-	25				NAC
P-S-RC-25x	600	25	-	36.70	385.0	524.0	NAC
P-L-RC-0[1]	2000	3	-				NAC
P-L-RC-25x	2000	25	-				NAC
M-E01-0[1]	600	5	-	39.10			NAC
M-E02-25x-RAC30[1]	600	5	-	36.73	377.7	594.8	RAC30
M-E04-0	600	25	-	39.10			NAC
M-E05-25x-RAC30	600	25	-	36.73			RAC30

[1] Accidental eccentricity reported for the axially loaded column

Solid elements C3D8 were used to represent the steel profile and concrete. The element meshes shown in Fig. 2 (b) were generated with a 15 mm element size. Steel reinforcements were simulated using T3D2 truss elements. The element mesh of the stirrups was generated using the edge-by-number resource, while the element mesh of the longitudinal reinforcement had an approximate dimension of 100 mm. The rigid plates were composed of discrete rigid parts with R3D4 rigid elements with approximate dimensions of 10 mm.

The interaction between the concrete and the steel rebars was simulated using the "Embedded Constraint", which is equivalent to assuming a perfect bond between the two materials. No experimental model showed any evidence of separation between the concrete and the steel web (Pereira *et al.* [10], Marques [14]). Also, the concrete restrained the steel web, avoiding the occurrence of local instabilities. Thus, the tie constraint was used to define the interaction property between the concrete on both sides and the steel web. Contrarily, the steel flanges are free to buckle outward due to local instabilities. Surface-to-surface contact was defined between the concrete and the steel flanges. The normal behavior was simulated using the "Hard contact" option, while the tangential behavior was defined using the "Penalty" option employing a friction coefficient of 0.3. The Newton-Raphson solution

strategy was employed to solve the numerical simulation, along with a line-search algorithm to enhance convergence. The geometrical non-linearities were enabled in the solution step.

2.2 Materials constitutive models

The non-linear behavior of materials was considered. Perfect plastic behavior was adopted for the steel profile and steel rebars. The Concrete Damaged Plasticity (CDP) model was selected to represent the behavior of concrete. The five plasticity parameters, dilation angle, eccentricity, biaxial-to-axial compression strength ratio, the ratio between the distances from the hydrostatic axis to the compression and tensile meridians, and the viscosity parameter were assumed as 33º, 0.1, 1.16, 0.667, and 0, respectively. The uniaxial stress-strain model proposed by Carreira and Chu [16] and presented in Eq. 1 was used to describe the behavior of concrete under compression. In Eq. 1, ε_{c0} is the concrete compressive peak strain. Equation 2, proposed by the same authors, was used to obtain the β parameter for the NAC used by Pereira *et al.* [10]. For the NAC and RAC30 used by Marques [14] and RAC50 used by Oliveira [7], the β parameter was adjusted by trial-and-error to match the experimental stress-strain curves as shown in Fig. 3.

$$\sigma_c = f_c \frac{\beta(\varepsilon/\varepsilon_{c0})}{\beta - 1 + (\varepsilon/\varepsilon_{c0})^{\beta}} \tag{1}$$

$$\beta = \left(\frac{f_c}{32.4}\right) + 1.55;\ f_c\ in\ MPa \tag{2}$$

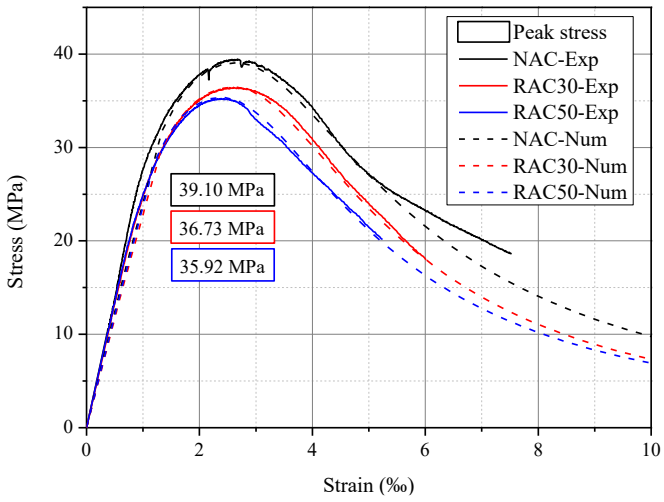


Figure 3 – Compression uniaxial stress-strain curves used for the concrete of Marques [14] and Oliveira [7]

The concrete tensile stress-strain curve was obtained using the Hordijk [17] model, as shown in Eq. 3. The maximum crack width (w_c) is determined by Equation 4, and the fracture energy (G_f) is obtained according to Eq. 5 (CEB 90[18]). Finally, the tensile inelastic strain is determined based on Eq. 6, in which l_{ch} is the characteristic element length. The damage parameter was determined according to the formulation proposed by Alfarah *et al.* [19].

$$\frac{\sigma_t}{f_t} = [1 + (3\,w/w_c)^3]e^{-6.93\frac{w}{w_c}} - 10\frac{w}{w_c}e^{-6.93} \tag{3}$$

$$w_c = 5.14\frac{G_f}{f_t} \tag{4}$$

$$G_f = G_{f0} \cdot \left(\frac{fcm}{10}\right)^{0.7} \tag{5}$$

$$\varepsilon_{in} = \frac{w}{l_{ch}} \tag{6}$$

3 Results and discussions

Figure 4 shows the Axial Load vs. Average axial strain curves for the calibration phase. The relative error (e) for the peak load prediction is shown for each curve. A negative error relates to an overestimation compared to the experimental result. The results in Fig. 4 show that the numerical model provides a good prediction of the experimental behavior both before and after the peak load. The model slightly overestimated the stiffness of the columns with RAC30. However, the higher discrepancy regarding the specimen M-E05-25x-RAC30 is attributed to the lower stiffness observed in the experiment. The model also yielded good predictions for the peak loads, with a relative error of less than 5%.

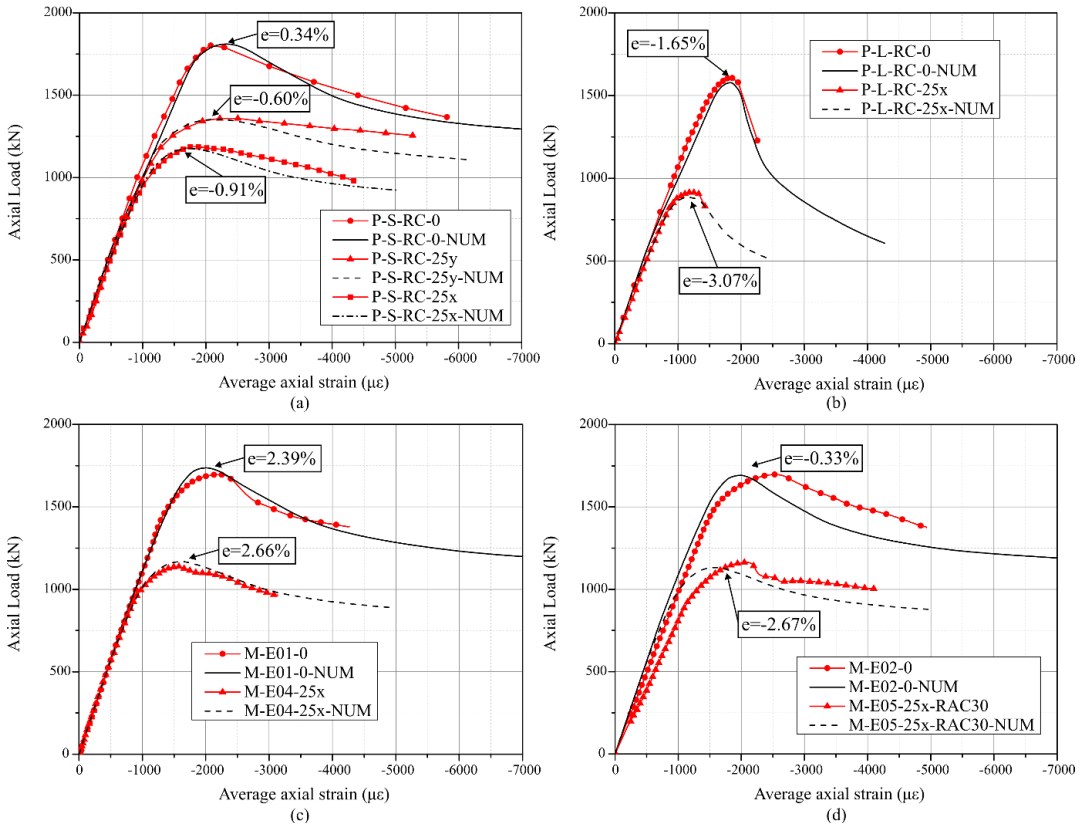


Figure 4 – Calibration results: (a) short specimens from Pereira *et al.* [20], (b) long specimens from Pereira *et al.*[14], (c) specimens with NAC from Marques [14] and (d) specimens with RAC30 from Marques [14]

The impact of increasing the replacement ratio to 50% was investigated by implementing the stress-strain shown in Fig. 3 in the calibrated numerical model. Despite the stress-strain curve, the remaining properties of the models were based on the study of Marques [14]. Figure 5 presents the behavior of the columns with 600 mm and 2000 mm for the different replacement ratios. The results indicate an overall decrease in structural behavior, with a slight reduction in stiffness, peak load, and residual capacity. For columns with 5 mm eccentricity, the model indicated reductions of 2.59% and 4.14% for RAC30 and RAC50 in 600 mm specimens, and 2.59% and 3.27% in 2000 mm specimens. Under 25 mm eccentricity, the reductions were 3.08% and 5.43% in 600 mm specimens, and 2.64% and 4.21% in 2000 mm specimens.

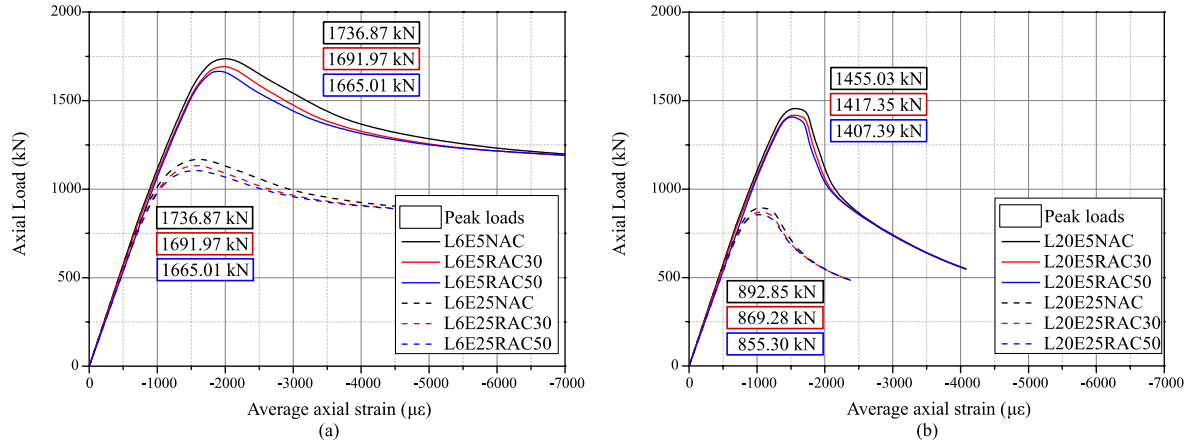


Figure 5 – Results for the variation of the replacement ratio: (a) 600 mm columns and (b) 2000 mm columns

4 Conclusions

This study presented a numerical investigation of partially encased composite columns produced with varying RCA replacement ratios. By using the calibrated model, it was observed that increasing the replacement up to 50% led to a slight reduction in the overall structural behavior of the column. The increase in slenderness associated with the rise in the replacement ratio did not result in any significant changes. The α_{AR} parameters for the RAC30 and RAC50, considering the mix proportions reported in the reference studies, are 0.13 and 0.22, respectively. Thus, the numerical results presented corroborate the recent guidelines that allow the replacement ratio with α_{AR} less than 0.2 without a significant change in the structural performance of the concrete.

Acknowledgements. This work was supported by the Brazilian Council For Scientific and Technological Development (CNPq) [grant number 140965/2022-0] and the Coordination of Superior Level Staff Improvement (CAPES).

Authorship statement. The authors hereby confirm that they are the sole liable persons responsible for the authorship of this work, and that all material that has been herein included as part of the present paper is either the property (and authorship) of the authors, or has the permission of the owners to be included here.

References

[1] K. Kalinowska-Wichrowska, E. Pawluczuk, M. Bołtryk, J. R. Jimenez, J. M. Fernandez-Rodriguez, and D. Suescum Morales, "The Performance of Concrete Made with Secondary Products—Recycled Coarse Aggregates, Recycled Cement Mortar, and Fly Ash–Slag Mix," *Materials*, vol. 15, no. 4, Art. no. 4, Jan. 2022, doi: 10.3390/ma15041438.

[2] R. V. Silva, J. de Brito, and R. K. Dhir, "Properties and composition of recycled aggregates from construction and demolition waste suitable for concrete production," *Construction and Building Materials*, vol. 65, pp. 201–217, Aug. 2014, doi: 10.1016/j.conbuildmat.2014.04.117.

[3] European Committee for Standardization, "EN 1992-1-1: Design of concrete structures – Part 1-1: General rules and rules for buildings, bridges and civil engineering structures (Final Draft FprEN 1992-1-1:2023)." 2023.

[4] Brazilian Association of Technical Standards, "NBR 15116: Recycled aggregates for uses in mortar and concrete - Requirements and test methods." 2021.

[5] J. Xiao, J. Li, and Ch. Zhang, "Mechanical properties of recycled aggregate concrete under uniaxial loading," *Cement and Concrete Research*, vol. 35, no. 6, pp. 1187–1194, Jun. 2005, doi: 10.1016/j.cemconres.2004.09.020.

[6] M. Turi Gerin, A. Sales, and S. De Nardin, "Mechanical and physical properties of recycled aggregates concrete," *Rev Tecnol*, vol. 29, no. 1, pp. 259–274, Jan. 2020, doi: 10.4025/revtecnol.v29i1.51289.

[7] F. G. B. S. Oliveira, "Análise experimental e numérica do comportamento à flexão de vigas formadas por perfis de aço parcialmente revestidas com concreto de resíduos reciclados de concreto," Master's Thesis, Universidade de São Paulo, 2022. doi: 10.11606/D.18.2022.tde-19102022-122217.

[8] A. Adessina, A. B. Fraj, J.-F. Barthélémy, and M. Gharbi, "Failure mechanism in recycled sand mortars and recycled aggregate concretes: Experimental and multiscale approaches," *Journal of Building Engineering*, vol. 101, p. 111882, May 2025, doi: 10.1016/j.jobe.2025.111882.

[9] Z. Liu, Y.-G. Zhao, L. Ma, and S. Lin, "Review on high-strength recycled aggregate concrete: Mix design, properties, models and structural behaviour," *Structures*, vol. 64, p. 106598, Jun. 2024, doi: 10.1016/j.istruc.2024.106598.

[10] M. F. Pereira, S. D. Nardin, and A. L. H. C. El. Debs, "Partially encased composite columns using fiber reinforced concrete: experimental study," *Steel and Composite Structures*, vol. 34, no. 6, pp. 909–927, 2020, doi: 10.12989/SCS.2020.34.6.909.

[11] H. Wang, J. Li, and Y. Song, "Numerical Study and Design Recommendations of Eccentrically Loaded Partially Encased Composite Columns," *Int J Steel Struct*, vol. 19, no. 3, pp. 991–1009, Jun. 2019, doi: 10.1007/s13296-018-0179-7.

[12] M. Ebadi Jamkhaneh, M. Ahmadi, and P. Sadeghian, "Simplified relations for confinement factors of partially and highly confined areas of concrete in partially encased composite columns," *Engineering Structures*, vol. 208, p. 110303, Apr. 2020, doi: 10.1016/j.engstruct.2020.110303.

[13] B. Wu, S.-M. Jian, and X.-Y. Zhao, "Structural behavior of steel-concrete partially encased composite columns containing demolished concrete lumps under axial compression," *Engineering Structures*, vol. 197, p. 109383, Oct. 2019, doi: 10.1016/j.engstruct.2019.109383.

[14] B. B. Marques, "Estudo experimental e numérico de pilares mistos parcialmente revestidos com concreto de resíduos reciclados de concreto e fibras de aço," Mestrado em Estruturas, Universidade de São Paulo, São Carlos, 2022. doi: 10.11606/D.18.2022.tde-22112022-115211.

[15] J. Liang, L. Wang, W. Zou, and W. Li, "Compressive behavior of partially encased recycled aggregate concrete columns after exposure to elevated temperature," *Journal of Constructional Steel Research*, vol. 221, p. 108889, Oct. 2024, doi: 10.1016/j.jcsr.2024.108889.

[16] Domingo J. Carreira and Kuang-Han Chu, "Stress-Strain Relationship for Plain Concrete in Compression," *ACI Journal Proceedings*, vol. 82, no. 6, Jan. 1985, doi: 10.14359/10390.

[17] HORDIJK, D. A, "Local approach to fatigue of concrete.," (Doctorate Thesis), Technische Universiteit Delft, Delft, 1991.

[18] Euro-International Committee for Concrete and Fédération internationale de la précontrainte, Eds., *CEB-FIP model code 1990: design code*, Repr. London: Telford, 1998.

[19] B. Alfarah, F. López-Almansa, and S. Oller, "New methodology for calculating damage variables evolution in Plastic Damage Model for RC structures," *Engineering Structures*, vol. 132, pp. 70–86, Feb. 2017, doi: 10.1016/j.engstruct.2016.11.022.

[20] M. F. Pereira, S. D. Nardin, and A. L. H. C. E. Debs, "Structural behavior of partially encased composite columns under axial loads," *Steel and Composite Structures*, vol. 20, no. 6, Art. no. 6, Jan. 2016.